

PAPER • OPEN ACCESS


Integrating microdosimetric *in vitro* RBE models for particle therapy into TOPAS MC using the MicrOdosimetry-based modeliNg for RBE ASsessment (MONAS) tool

To cite this article: Giorgio Cartechini *et al* 2024 *Phys. Med. Biol.* **69** 045005


View the [article online](#) for updates and enhancements.

You may also like

- [The influence of RBE variations in a clinical proton treatment plan for a hypopharynx cancer](#)
N Tilly, J Johansson, U Isacson et al.
- [A comparison of the relative biological effectiveness of low energy electronic brachytherapy sources in breast tissue: a Monte Carlo study](#)
Shane A White, Brigitte Reniers, Evelyn E C de Jong et al.
- [Impact of uncertainties in range and RBE on small field proton therapy](#)
Maria Marteinsdottir, Jan Schuemann and Harald Paganetti



Joining forces:
One complete
QA solution for
Dosimetry with
myQA[®], QUASAR[™]
and Radcal[®]!



The diagram is a circular graphic with four colored segments: Machine QA (dark blue), Patient Specific QA (green), Medical Imaging QA (light blue), and Risk Management (pink). In the center of the circle is a wireframe human head. The background of the entire advertisement is dark with a pattern of small, colorful dots.



PAPER

OPEN ACCESS

RECEIVED
17 July 2023REVISED
24 November 2023ACCEPTED FOR PUBLICATION
11 January 2024PUBLISHED
5 February 2024

Original content from this work may be used under the terms of the [Creative Commons Attribution 4.0 licence](#).

Any further distribution of this work must maintain attribution to the author(s) and the title of the work, journal citation and DOI.



Integrating microdosimetric *in vitro* RBE models for particle therapy into TOPAS MC using the MicrOdosimetry-based modeliNg for RBE ASsessment (MONAS) tool

Giorgio Cartechini^{1,2} , Marta Missiaggia^{1,2} , Emanuele Scifoni² , Chiara La Tessa^{1,2,3} and Francesco G Cordoni^{2,4}

¹ Department of Radiation Oncology, University of Miami Miller School of Medicine, 1550 NW 10th Avenue, 33126, Miami (FL), United States of America

² Trento Institute for Fundamental Physics and Application (TIFPA), via Sommarive 15, I-38123, Trento, Italy

³ Department of Physics, University of Trento, via Sommarive 14, I-38123, Trento, Italy

⁴ Department of Civil, Environmental and Mechanical Engineering, University of Trento, via Mesiano 77, I-38123, Trento, Italy

E-mail: francesco.cordoni@unitn.it

Keywords: microdosimetry, RBE, Monte Carlo, TOPAS MC, treatment planning, particle therapy, radiation biophysical modeling

Supplementary material for this article is available [online](#)

Abstract

Objective. In this paper, we present MONAS (MicrOdosimetry-based modellNg for relative biological effectiveness (RBE) ASsessment) toolkit. MONAS is a TOPAS Monte Carlo extension, that combines simulations of microdosimetric distributions with radiobiological microdosimetry-based models for predicting cell survival curves and dose-dependent RBE. **Approach.** MONAS expands TOPAS microdosimetric extension, by including novel specific energy scorers to calculate the single- and multi-event specific energy microdosimetric distributions at different micrometer scales. These spectra are used as physical input to three different formulations of the *microdosimetric kinetic model*, and to the *generalized stochastic microdosimetric model* (GSM²), to predict dose-dependent cell survival fraction and RBE. MONAS predictions are then validated against experimental microdosimetric spectra and *in vitro* survival fraction data. To show the MONAS features, we present two different applications of the code: (i) the depth-RBE curve calculation from a passively scattered proton SOBP and monoenergetic ¹²C-ion beam by using experimentally validated spectra as physical input, and (ii) the calculation of the 3D RBE distribution on a real head and neck patient geometry treated with protons. **Main results.** MONAS can estimate dose-dependent RBE and cell survival curves from experimentally validated microdosimetric spectra with four clinically relevant radiobiological models. From the radiobiological characterization of a proton SOBP and ¹²C fields, we observe the well-known trend of increasing RBE values at the distal edge of the radiation field. The 3D RBE map calculated confirmed the trend observed in the analysis of the SOBP, with the highest RBE values found in the distal edge of the target. **Significance.** MONAS extension offers a comprehensive microdosimetry-based framework for assessing the biological effects of particle radiation in both research and clinical environments, pushing closer the experimental physics-based description to the biological damage assessment, contributing to bridging the gap between a microdosimetric description of the radiation field and its application in proton therapy treatment with variable RBE.

1. Introduction

Proton therapy is now widely recognized as an advanced form of radiation therapy compared to the conventional use of photons for treating a steadily increasing number of types of cancers, especially deep-seated, radioresistant, and hypoxic (Loeffler and Durante 2013, Tambas *et al* 2022). The advantages of ions over photons are mainly attributed to the localized energy deposition at the end-of-range of the particle, known as the Bragg

peak, resulting in a highly conformal dose distribution and normal tissue sparing (Durante *et al* 2017). In addition to the physical advantages, ion beam therapy is characterized by larger biological effectiveness. The reason for this is the higher ionization density and more severe damage to cellular DNA (e.g. double-strand breaks and clustered damage) than photon radiation (Scholz *et al* 2001). The superior biological effectiveness of ions is quantified by the *relative biological effectiveness* (RBE), that is, the ratio between the reference radiation and the ion dose causing a same biological effect (Jäkel *et al* 2016). In particle therapy, in general, to obtain a homogeneous biological effect in the tumor volume, the RBE of ions is included in the treatment plan optimization as a multiplication factor to the absorbed physical dose. In proton treatment planning, an RBE value equal to 1.1 is adopted for both tumor and normal tissue, namely, protons are considered 10% more effective than photons. Despite the clinical practice assumes a spatially invariant RBE for protons, pre-clinical *in vitro* and *in vivo* studies have demonstrated that a constant RBE is an oversimplification due to its dependence on numerous parameters (dose, dose rate, cell line, biological endpoint, radiation quality in the specific voxel, etc) (Paganetti and Goitein 2000, Paganetti 2014), with the RBE being significantly above 1.1 in the distal region, (Missiaggia *et al* 2020). For heavier ions like Carbon and Helium, the variations in RBE along the beam penetration depth are so significant that a fixed RBE value cannot be deemed appropriate, and current treatment plans are calculated accounting for a variable RBE (Inaniwa and Kanematsu 2018, Mairani *et al* 2022).

Therefore, for optimal treatment outcomes that effectively balance the targeting of the tumor and the minimization of the damage to the surrounding healthy tissue, it is crucial to accurately estimate the RBE at any point of the irradiated field. The first step in achieving such a challenging goal is to characterize the radiation field, both in terms of macroscopic absorbed energy and the microscopic local pattern of energy deposition. Microdosimetry (Zaider *et al* 1996) has proven over the years to be an extremely powerful tool to accomplish such a task. Microdosimetry is a branch of physics that studies the energy deposition of particles at a scale in the order of a few microns, which is the scale of a cell nucleus, believed to be the most sensitive target to radiation-induced cell killing due to the presence of DNA. At the micron scale, single-particle energy deposition is characterized by large fluctuations due to the inherently stochastic nature of particle interaction, and, therefore, microdosimetry characterizes the radiation field in terms of probability distributions of energy.

By characterizing the energy depositions at the micron scale, microdosimetry provides an ideal tool to link radiation to its biological effects directly. For this reason, many radiobiological models rely on microdosimetry principles, among which the microdosimetric kinetic model (MKM) is the most prominent and widespread in particle therapy (Hawkins 1994, 1996, Inaniwa and Kanematsu 2018).

The MKM is a mechanistic model that predicts the cell survival fraction of irradiated cells based on microdosimetric average values and estimates the resulting RBE (Zaider *et al* 1996). In particular, the MKM predicts the logarithm of the cell survival fraction of irradiated cells as a linear-quadratic (LQ) function of the imparted dose, (McMahon 2018)

$$\log S(D) = -\alpha D - \beta D^2, \quad (1)$$

with α and β two radiobiological parameters that depend on the biological tissue and on the specific ionizing radiation. Despite the MKM has displayed notable consistency with experimental data obtained both *in vitro* and *in vivo* (Mein *et al* 2020), over time, numerous successive adaptations of the MKM have been developed in the literature, (Kase *et al* 2006, 2007, Sato *et al* 2006, Inaniwa *et al* 2010, Bellinzona *et al* 2021a), primarily aimed to address limitations of the original model in specific scenarios where its underlying assumptions were unsuitable. Currently, the MKM represents the standard model used to calculate the RBE in several carbon-ion therapy centers, (Mein *et al* 2020), and, along with the Local Effect Model (LEM), the MKM is one of the only two models currently used in clinics for this purpose. Further, the MKM has been used as the reference RBE model in the recently first treated patient with helium, (Mairani *et al* 2022). The MKM's success and widespread use highlight the importance of microdosimetry in accurately predicting the biological effects of radiation and optimizing treatment planning for patients.

Recently, the *generalized stochastic microdosimetric model* (GSM²) has been developed, (Cordoni *et al* 2021), which is a theoretically grounded mechanistic radiobiological model able to include several spatiotemporal stochastic effects inherent to the formation and repair of radiation-induced DNA damage, (Cordoni *et al* 2022a, 2022b, Missiaggia *et al* 2023b). GSM² is a fully probabilistic model that overcomes one of the main assumptions shared by most existing radiobiological models including the MKM, that is the fact that the distribution of the number of damages induced by radiation on DNA is Poissonian. In doing so, GSM² describes the time evolution of probability distribution of radiation-induced DNA damage rather than focusing on average values as done in the MKM.

Although mechanistic models based on the microdosimetric description of radiation field quality have been shown as an accurate tool for predicting RBE in ion therapy, experimental microdosimetric spectra are still challenging to measure in the daily clinical practice even using commercial detectors, e.g. tissue equivalent proportional counter (TEPC) or silicon-on-insulator (SOI) detector (Bradley *et al* 2001, Kase *et al* 2006,

Rosenfeld 2016, Conte *et al* 2020, Missiaggia *et al* 2020, Missiaggia *et al* 2021, 2023a). Therefore, numerical algorithms, such as Monte Carlo (MC) particle simulation toolkits, have been demonstrated as a valuable alternative for the microdosimetric characterization of the radiation field (Zhu *et al* 2019, Baratto-Roldán *et al* 2021, Missiaggia *et al* 2020, 2023a). Nevertheless, MC simulations for microdosimetric spectra are exceedingly time-consuming, which has prevented their integration into clinical treatment planning systems. This limitation has hindered the utilization of valuable microdosimetric insights within the clinical practice. Hence, to expedite computational processes, various numerical approximations have been incorporated into MKM models, Inaniwa and Kanematsu (2018), enabling their practical application in everyday scenarios. The most relevant one was the use of an analytical amorphous track model of particle energy deposition at the nanometer and micrometer scale (Kiefer and Straaten 1986, Chatterjee and Schaefer 1976), which speed up the computation of microdosimetric quantities used as input for the MKM RBE models (Kase *et al* 2007, Inaniwa and Kanematsu 2018). It is important to note that in addition to microdosimetry, nanodosimetry holds great promise in shedding light on the biological effects of radiation. Over the years, several radiobiological models have been proposed to establish connections between ionization cluster size and the formation of DNA lesions (Garty *et al* 2010, Rabus and Nettelbeck 2011). Notably, (Conte *et al* 2018, Selva *et al* 2020), nanodosimetry offers a direct pathway to understanding the biological consequences of radiation exposure. Furthermore, it has become evident that both microdosimetric and nanodosimetric scales play a significant role in assessing radiation-induced biological damage (Friedrich *et al* 2018, Baiocco *et al* 2022). However, it is crucial to highlight that accurately simulating nanoscale phenomena necessitates the implementation of a physics list based on track structure, which, for the sake of clarity, is not the focus of this paper.

In this work, we present a novel TOPAS Monte Carlo (MC) microdosimetric extension: MicrOdosimetry-based modelling for RBE ASsessment (MONAS). MONAS combines full MC simulations of microdosimetric spectra with clinically relevant microdosimetry-based radiobiological models for cell survival and dose-dependent RBE assessment. Furthermore, by utilizing the new scorers of MONAS, it is now possible to generate fully Monte Carlo-based Look-Up tables (LUTs) of radiobiological parameters α and β for RBE-based treatment plan optimization in clinical proton therapy. MONAS is based on the existing TOPAS microdosimetric extension (Zhu *et al* 2019), which models the main microdosimetry detectors used in literature and scores the lineal energy distributions. The lineal energy y is defined as the energy ϵ deposited over the target volume mean chord length l , i.e. $y = \epsilon/l$. This is the quantity of reference measured in experimental microdosimetry. Starting from the simulated y distributions, we implemented a novel scorer based on specific energy z , defined as the energy imparted ϵ over the mass m of sensitive volume, i.e. $z = \epsilon/m$. The extension allows the user to calculate specific energy distributions at different microscopic scales. These z distributions are the building blocks for the microdosimetry-based radiobiological models implemented in MONAS. We included the GSM² and three clinically relevant MKM formulations: saturation corrected MKM (MKM- z^*) (Kase *et al* 2006), double stochastic MKM (DSMKM) (Sato and Furusawa 2012) and the modified Stochastic MKM (mSMKM) (Inaniwa and Kanematsu 2018). Therefore, MONAS predicts dose-dependent cell survival fraction and RBE specifically for the simulated radiation field.

MONAS simulates experimental microdosimetric distributions acquired with three different detectors, and from validated z -distributions, it calculates cell survival curves which can be directly compared with experimental *in vitro* data. Therefore, MONAS is the first full MC toolkit that allows the user to benchmark the physical input and the biological output of the radiobiological models with experiments. To show that, we compared the MONAS cell survival curves with experimental data from the particle irradiation data ensemble (PIDE) (Friedrich *et al* 2013). We also calculated cell survival and RBE depth curves using all radiobiological models available in MONAS for a proton spread-out Bragg-peak (SOBP), whose microdosimetric spectra were previously measured by us (Missiaggia *et al* 2023a) and used to validate TOPAS. Additionally, to test the model predictions for heavy ions, we characterized a 300 MeV/u ¹²C-ion Bragg curve in water (Martino *et al* 2010, Burigo *et al* 2013).

MONAS is also an accurate and fast tool to predict RBE in proton therapy treatment plans. In particular, in this study, we used the MONAS extension to generate full Monte Carlo-based Look-Up-tables (LUTs) of radiobiological parameters α and β from monoenergetic proton beams. By combining MONAS LUTs and TOPAS MC's precision in tracking therapeutic protons within the patient's anatomy, MONAS allows the calculation of the RBE spatial distribution in a real patient's geometry. In particular, we determined the mixed-filed α_{mix} and $\sqrt{\beta_{\text{mix}}}$, defined as the dose-averaged of single particle α and $\sqrt{\beta}$ extrapolated from MONAS LUTs, in each voxel of the scoring mesh. Consequently, we could predict the biological effectiveness of a real proton beam. As an example, we recalculated with TOPAS MC a real head and neck proton treatment, optimized with the Eclipse planning system (Varian Medical Systems, Palo Alto, CA) and delivered at the Dvoskin Proton Therapy Center (University of Miami). Our study demonstrated that by fully integrating the MONAS toolkit within the TOPAS MC code, we can accurately simulate microdosimetric spectra and use them

as input for the microdosimetry base models, enabling us to estimate the effect of radiation on biological tissue in clinical conditions. The present work represents the first crucial step toward bridging the gap between microdosimetry and clinical applications. By providing a comprehensive microdosimetric analysis of the radiation field, we show how real-life clinical and experimental scenarios can greatly benefit, allowing clinicians and researchers to estimate the biological effect of radiation accurately.

The main contributions of the present paper are:

- (i) to introduce a Monte Carlo-based microdosimetric toolkit that allows estimating *in vitro* cell survival data and RBE distribution in realistic radiotherapy treatment plans with a full microdosimetric description of radiation.
- (ii) to introduce a new methodology for utilizing the microdosimetry-based radiobiological models to evaluate RBE in real proton therapy treatments.

2. Material and methods

2.1. Microdosimetric quantities and microdosimetry-based RBE models

Microdosimetry considers two quantities of interest: the *specific energy* z and *lineal energy* y (Zaider *et al* 1996).

The *specific energy* z is the ratio between the energy imparted by ionizing radiation ϵ and the mass m of the sensitive volume,

$$z = \frac{\epsilon}{m}.$$

The *lineal energy* y is the ratio between the energy imparted by ionizing radiation ϵ and the mean chord length of the sensitive volume l ,

$$y = \frac{\epsilon}{l}.$$

It is possible to relate y to z via the following relation $z = \frac{l}{m}y$. By assuming a spherical site of density $\rho = 1 \text{ g cm}^{-3}$ and radius r expressed in μm , the relations between the y and z is:

$$z [\text{Gy}] = \frac{0.16}{\pi \cdot \rho [\text{g/cm}^3] \cdot r^2 [\mu\text{m}^2]} y [\text{keV}/\mu\text{m}] \quad (2)$$

where 0.16 is the coefficient to pass from keV/g to Gy.

The lineal energy y is the reference quantity in experimental microdosimetry, whereas the specific energy z is the main reference quantity in microdosimetry-based radiobiological models. A key difference between lineal energy and specific energy is that the quantity ϵ refers to the energy imparted in a single event for y , or the energy imparted in any number of events for z . This implies that when considering the distribution of z , the ionization of more than one event must be considered. For this reason, most of the MKM and the GSM² models are based on the so-called *multi-event* specific energy distributions (Bellinzona *et al* 2021b, Zaider *et al* 1996).

As standard in microdosimetry, the first two moments of the single-event distribution play a crucial role and they are defined as

$$\bar{z}_F = \int_0^\infty z f_1(z) dz, \quad (3)$$

$$\bar{z}_D = \frac{1}{\bar{z}_F} \int_0^\infty z^2 f_1(z) dz. \quad (4)$$

The most used microdosimetry-based radiobiological model is the MKM. It utilizes a system of differential equations to predict the survival fraction of irradiated cells. These equations describe the time evolution of the average number of DNA damages that can be repaired if they lead to cell death. To better align with biological data, the MKM postulates that the nucleus is partitioned into sub-units called *domains* so that the number of DNA damages is evaluated for each domain separately. Therefore, the probability of cell survival is estimated by considering all the domains into which the nucleus has been divided.

Since its original formulation in Hawkins (1994), the MKM has been widely generalized to include several endpoints and stochastic inter- and intra-cellular effects, (Hawkins 1996, 2003, Inaniwa *et al* 2010, Manganaro *et al* 2017, Inaniwa and Kanematsu 2018, Bellinzona *et al* 2021b, Attili *et al* 2022).

A proposed correction to the MKM model, named saturation corrected MKM (MKM- z^*), aims to improve its alignment with heavy ion data, which exhibits the so-called *overkill effect* (Kase *et al* 2006). This effect consists in a decrease of the RBE versus LET, for LET beyond approximately $150 \text{ keV } \mu\text{m}^{-1}$, following its initial raise for increasing LET (Kase *et al* 2006). Although the saturated corrected MKM shows a better match with

experimental data, it still does not include energy deposition variations both at the cell domain and nucleus level. To include these effects, the double stochastic MKM (DSMKM) has been proposed (Sato and Furusawa 2012). In the same work, the authors proposed an approximation of the DSMKM, named stochastic MKM (SMKM). It was developed to reduce the computational time by approximating the stochastic nature of z at the cell domain level with its mean value and variance. The SMKM has been further simplified in Inaniwa and Kanematsu (2018) to speed up the computational time and to be implemented in treatment planning systems. The modified version of SMKM (mSMKM) is based on the assumption that, in charged-particle therapy, the domain-specific energy z_d is, in general, delivered by a large number of low-energy deposition events, and the events inducing the saturation of complex DNA damages are rare. Also, it is assumed that the specific energy imparted z_n is sufficiently close to the macroscopic dose D . From these hypotheses, an analytical formulation of the cell survival fraction as a function of domain and nucleus-specific energies was derived.

Recently, starting from the building assumptions of the MKM, a novel microdosimetry-based radiobiological model, GSM², was presented, (Cordoni *et al* 2021, 2022a, 2022b). GSM² aims at providing a fully probabilistic model that takes into account the effects of stochasticity in different aspects of radiation-induced damage, e.g. in the initial damage distribution as well as damage evolution.

Like the MKM formulations, GSM² describes the time evolution of DNA lesions in a cell nucleus, which is divided into smaller sub-domains. Differently from the MKM, GSM² can describe the time evolution of the whole probability distribution of lesions rather than simple average values. Notable enough, it has been shown in (Cordoni *et al* 2022b, Missiaggia *et al* 2023b), that the distribution of lesions predicted by GSM² can deviate from a Poisson distribution, as assumed by the MKM models, especially at sufficiently high LET and doses.

Supplementary materials provide a detailed description of the microdosimetric quantities, formalism, and the radiobiological models presented in this work.

2.2. TOPAS

The microdosimetry-based radiobiological extension presented in this work extends the TOPAS MC toolkit (Perl *et al* 2012). TOPAS is an easy-to-use interface to the Geant4 Simulation toolkit (Agostinelli *et al* 2003) allowing both medical physicists and researchers to make Monte Carlo simulations without the necessity of advanced coding knowledge. In Zhu *et al* (2019) the microdosimetric extension of TOPAS has been implemented, allowing to score of lineal energy y with three different types of detectors: (i) spherical Tissue Equivalent Proportional Counter (TEPC), (ii) a cylindrical TEPC (also known a mini-TEPC) and (iii) Silicon on Insulator (SOI) microdosimeter. These detectors are the reference detectors for microdosimetry, (Bradley *et al* 2001, De Nardo *et al* 2004, Debrot *et al* 2018, Bianchi *et al* 2022, Missiaggia *et al* 2020, 2023a). The microdosimetric extension offers to the user the possibility to save microdosimetric spectra ($yf(y)$ and $yd(y)$) and the relative average quantities (y_F and y_D) for each detector, including the contribution of the particle species of the radiation field. The lineal energy distributions obtained via the TOPAS microdosimetric extension have been benchmarked with experimental data, showing good agreement, (Zhu *et al* 2019, Missiaggia *et al* 2023a).

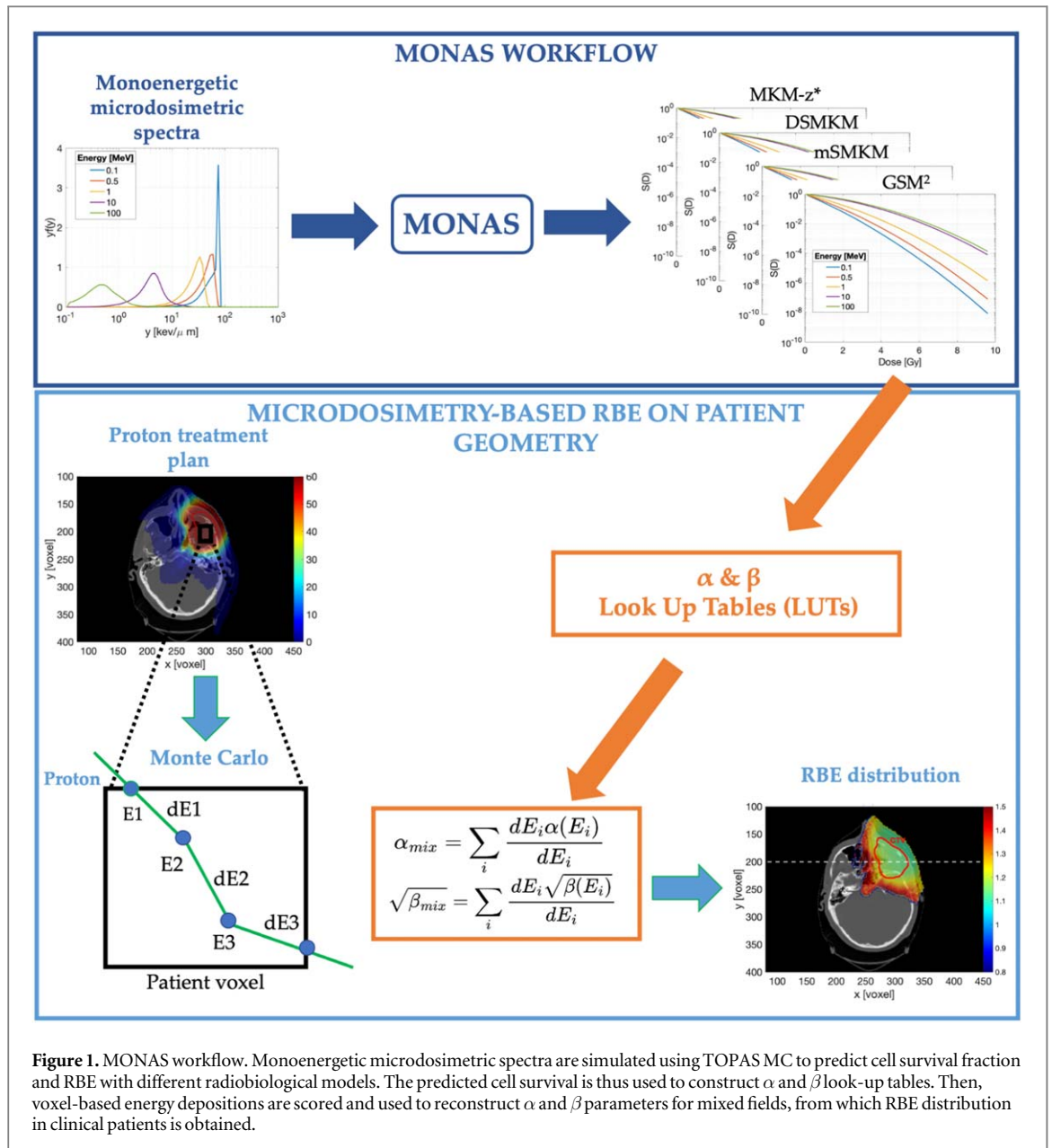
2.2.1. MONAS

MONAS extension starts from the original lineal energy scorer to provide a further toolkit that calculates specific energy z . Based on specific energy microdosimetric spectra, MONAS predicts cell survival fraction and RBE using the different MKM formulations and GSM² radiobiological model. The workflow of MONAS is depicted in figure 1.

In addition to the parameters of the lineal energy scorer (Zhu *et al* 2019), new optional parameters were implemented to activate the cell-survival and RBE calculations module according to MKM and GSM²: *GetRBEWithMKModel*, *GetRBEWithGSM2*. The user can further choose one or more MKM formulations available by setting the value of the string parameter *MKMCalculation* equal to (i) 'MKM-z*' for the saturation corrected MKM, (ii) 'mSMKM' for the modified-SMKM or (iii) 'DSMKM' for the double stochastic MKM. By default, the saturation corrected is set. The cell-survival S is computed as a function of macroscopic absorbed dose D , given as input parameter by the user setting the parameter *SurvivalDoses*; thus, RBE values are calculated as a function of $S(D)$ as follows

$$\text{RBE}(S, D) = \frac{\sqrt{\alpha_X^2 - 4\beta_X \ln(S(D))} - \alpha_X}{2\beta_X D}, \quad (5)$$

where α_X and β_X are the linear-quadratic coefficients of photon reference radiation. Model-specific radiobiological parameters can be set both for MKM and GSM² separately, including the reference radiation coefficients for the RBE calculations. Table 1 summarizes all MONAS parameters and their default values. Further details about the evaluation of radiobiological parameters will be given in section 2.3.1.



The output files include the values set by the user both for the radiobiological model and reference radiation, specific energy spectra both for cell nucleus and domain, cell survival for the macroscopic doses specified, and RBE as a function of cell irradiation dose in ASCII format. The MONAS extension is an open-source code available on GitHub (Cartechini 2023).

2.2.2. Specific energy spectra

Parallel to the default lineal energy scorer, MONAS includes the calculation of specific energy quantities converting *single-event* lineal energy y into *single-event* specific energy z_1 according to the equation (2). *Single-event* and *multi-event* specific energy spectra are calculated and used for cell survival and RBE evaluation (Supplementary Materials). By setting the boolean parameter *SaveSpecificEnergySpectra*, the user can save in ASCII format the *single-event* and *multi-event* distributions calculated on cell domain and cell nucleus: $z_{x,F} f_{x,1}(z_x)$, $z_x f_{x,1}(z_x)$, $z_x f_x(z_x, D/z_{d,F})$, where the subscript x can be either d for the domain and n for the nucleus distributions.

Since the n -fold convolution for the *multi-event* calculation is time-consuming, especially for high doses when the number of convolutions increases, a Monte Carlo approach for evaluating the *multi-event* distribution has been specifically implemented according to the following workflow: (i) the number of tracks k which deposit energy on sensitive volume is generated from a Poisson distribution with mean value $\lambda_n = z_n/z_{d,F}$ for cell domain and $\lambda_n = D/z_{n,F}$ for nucleus, respectively. Then, (ii) k *single-event* specific energies z_1 are sampled from the single-event probability distribution $f_1(z)$ and summed up to obtain the total specific energy $z_{tot} = \sum_{i=1}^k z_{1,i}$ deposited in the target; (iii) the *multi-event* probability distribution $f(z, \lambda_n)$ both for cell domain and the nucleus

Table 1. Summary of new input parameters for survival, RBE, and quality factor scorers. The parameter types are indicated according to the TOPAS syntax (*b* stands for boolean, *sv* for string vector, *u* for unitless double, *i* for integer). Default model-specific biological parameters refer to the HSG cell line.

Parameter	Type	Default	Note
<i>GetRBEWithMKM</i>	b	True	Flag for Survival and RBE calculation with MKM
<i>MKMCalculation</i>	sv	MKM-z*	String vector with MKM formulations: “MKM-z*”, “mSMKM”, ‘DSMKM’
<i>MKM_Alpha0</i>	u	0.13 Gy ⁻¹	MKM parameters
<i>MKM_Beta0</i>		0.05 Gy ⁻²	
<i>MKM_AlphaX</i>		0.19 Gy ⁻¹	
<i>MKM_BetaX</i>		0.05 Gy ⁻¹	
<i>MKM_rho</i>		1 gcm ⁻³	
<i>MKM_y0</i>		150 keV μm ⁻¹	
<i>MKM_DomainRadius</i>		0.44 μm	
<i>MKM_NucleusRadius</i>		8.0 μm	
<i>GetRBEWithGSM2</i>	b	false	Flag for Survival and RBE calculation with GSM ²
<i>GSM2_AlphaX</i>	u	0.19 Gy ⁻¹	GSM ² model parameters
<i>GSM2_BetaX</i>		0.05 Gy ⁻²	
<i>GSM2_rho</i>		1 g cm ⁻³	
<i>GSM2_a</i>		0.037 h ⁻¹	
<i>GSM2_b</i>		0.182 h ⁻¹	
<i>GSM2_r</i>		3.641 h ⁻¹	
<i>GSM2_DomainRadius</i>		0.8 μm	
<i>GSM2_NucleusRadius</i>		5.0 μm	
<i>SetMultieventStatistic</i>	i	10 ⁴	Number of iterations for calculating the <i>multi-event</i> probability distribution via Monte Carlo approach
<i>SaveSpecificEnergySpectra</i>	b	False	Flag for saving in an ASCII file the <i>single</i> — and <i>multi-event</i> distributions for cell domain and nucleus

is thus constructed by iterating steps (i) and (ii) N-times according to the parameter *SetMultieventStatistic*. A scheme of the algorithmic construction described is depicted in figure 2.

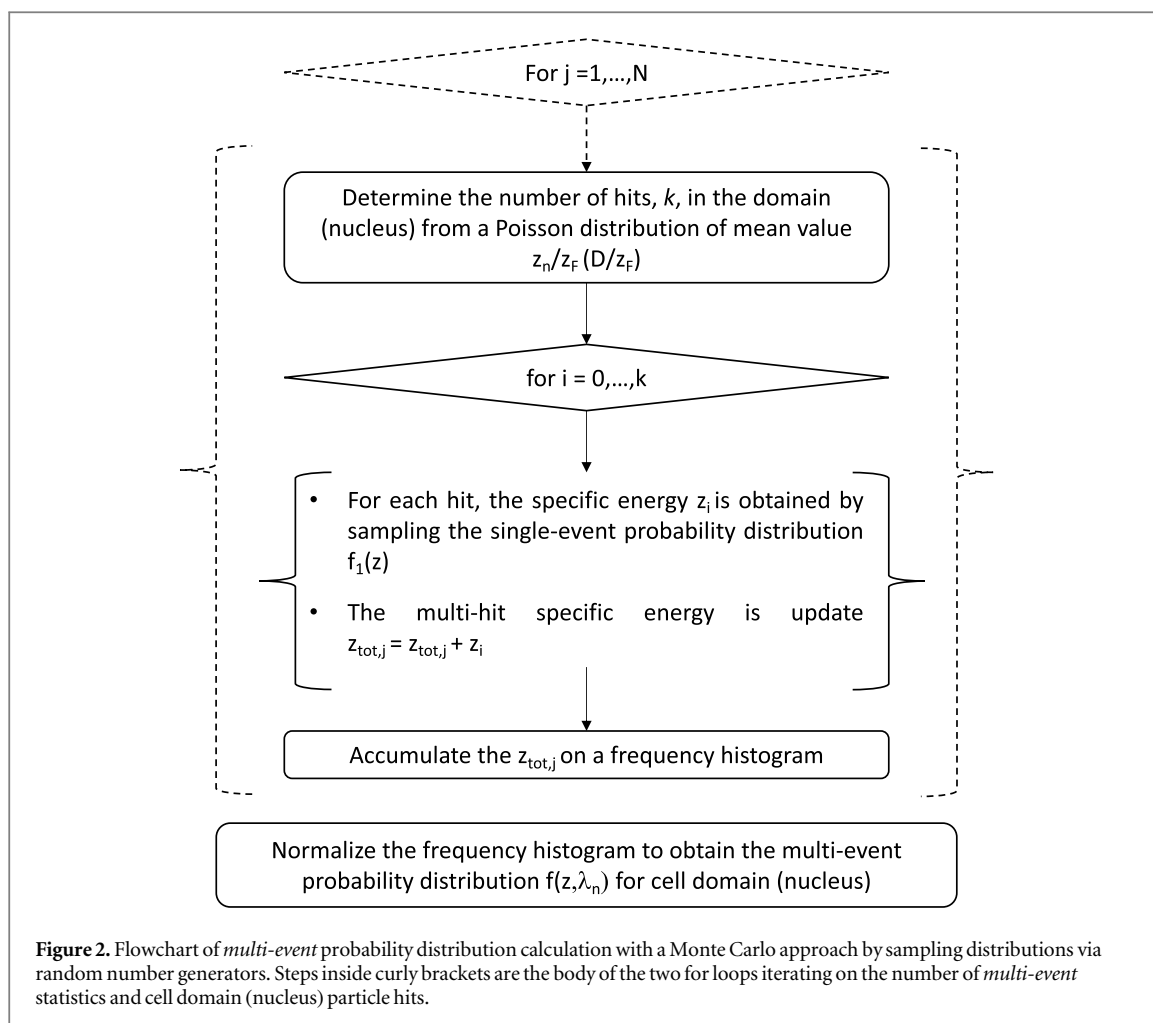
2.3. Cell-survival and RBE

The main feature of the MONAS extension is the prediction of cell survival curves and dose-dependent RBE after irradiation with ion beams. To prove the accuracy of the toolkit, we determined the radiobiological parameters specific to each model by comparing the survival predictions with experimental *in vitro* data on the human salivary gland (HSG) cell line. Once the model parameters were determined, we used MONAS to predict RBE distribution in two relevant cases for proton therapy: passively scattering proton spread-out Bragg peak (SOBP) (Tommasino *et al* 2019, Missiaggia *et al* 2023a) and head and neck proton therapy irradiation delivered at the Dvoskin Proton therapy center (University of Miami) and optimized with the Eclipse treatment planning system (Varian Medical Systems, Palo Alto, CA).

2.3.1. Radiobiological parameters

The radiobiological models implemented in this work are based on a variable number of free parameters independent of the radiation type, but they are only cell-line dependent.

These parameters were estimated by fitting the models with *in vitro* cell-survival experimental curves available in the literature and measured for a specific irradiation condition. It is worth stressing that, previous works (Kase *et al* 2006, Sato and Furusawa 2012, Inaniwa and Kanematsu 2018) reported MKM parameters for HSG cell line. Nonetheless, since the physical estimation of the radiation field is different from what was implemented in MONAS, the biological parameters have been fitted to ensure the highest reproducibility of *in vitro* cell survival experiments. In the present work, we characterized the radiation field regarding lineal energy and specific energy spectra by exploiting the TOPAS toolkit, a condensed history Monte Carlo algorithm. On the contrary, a different methodology was used both for the DSMKM and for the mSMKM (Sato and Furusawa 2012, Inaniwa *et al* 2013). DSMKM exploits a combination of microdosimetric Monte Carlo simulations with PHITS code (Sato *et al* 2013) in 1 μm volume for the cell domain (Sato *et al* 2009, 2006), while a Fermi function of macroscopic LET is used for evaluating the specific energy probability distribution on cell nucleus (Sato and Furusawa 2012). The modified-SMKM, instead, exploits analytical amorphous-track models to describe the radial dose distribution of the ion track and, thus, to compute the specific energy deposited on the cell domain and nucleus (Chatterjee and Schaefer 1976, Kiefer and Straaten 1986, Kase *et al* 2006, Inaniwa *et al* 2010). Due to the intrinsic difference in the description of radiation energy deposition in the sensitive volume between TOPAS and the previous work, we re-calculated the model parameters. A systematic comparison



between Monte Carlo condensed history (e.g. TOPAS MC) and track structure algorithm for calculating specific energy spectra is out of the scope of this work.

Therefore, the parameters for the MKM and GSM² were determined to reproduce *in vitro* experimental data of HSG cells. Experimental cell survival curves were taken from the Particle Irradiation Data Ensemble (PIDE) (Friedrich *et al* 2013) in which a large amount of cell survival data are systematically collected and analyzed as a function of particle LET, cell line, and reference radiation. Regarding the estimation of specific energy spectra, we simulated with TOPAS MC (v3.7) a water sphere placed in a vacuum world to avoid particle energy loss outside the sensitive volume. The sphere was irradiated by a mono-energetic ³He (10.2 MeV/u and 4.89 MeV/u) and ¹²C (12.9 MeV/u and 126 MeV/u) ion beams as reported in the experiments (Furusawa *et al* 2000, Friedrich *et al* 2013). The beam was modeled as the *Environment* particle source available in TOPAS. It creates an isotropic, uniform radiation field enclosing the water sphere. The default TOPAS physics list was used (Jarlskog and Paganetti 2008). Then, we scored the specific energy spectra in the sensitive volume. It must be remarked that the simulation setup used to reproduce the radiobiological data approximates the complexities of the experimental conditions. Based on beam energy information in the PIDE database, we assumed a purely mono-energetic beam as a particle source. This approximation can lead to deviations between predicted and experimental cell survival curves.

2.3.2. Cell survival and RBE for a proton Spread-out Bragg-peak

Recently in Missiaggia *et al* (2023a), a systematic characterization of the radiation field produced by passively scattered proton SOBP generated by a pencil beam of 148 MeV has been presented. Microdosimetric spectra were acquired with spherical TEPC both in-field and out-of-field. The same work also shows a good agreement between TOPAS microdosimetric simulations and experiments.

Starting from validated lineal energy spectra, we calculated cell survival, and RBE along the beam axis using the MONAS code. As described in Missiaggia *et al* (2023a), we simulated the Far West Technologies LET-1/2 spherical TEPC with an active volume made of pure propane gas (C₃H₈) at an operative pressure such that it is equivalent to a tissue sphere of 2 μm in diameter. The default physics list was used, and the particle production

cut was set according to the microdosimetric extension (Zhu *et al* 2019). About 10^7 primaries were simulated for each position along the beam axis. 200 kV x-ray was chosen as reference radiation for the HSG cell line, with $\alpha_X = 0.19 \text{ Gy}^{-1}$ and $\beta_X = 0.05 \text{ Gy}^{-2}$ (Kase *et al* 2006).

2.3.3. Cell survival and RBE for a ^{12}C -ion Bragg-peak

We simulated a 300 MeV/u ^{12}C -ion Bragg curve to test the MONAS toolkit with heavy ion irradiation. The simulation geometry described in Zhu *et al* (2019), Burigo *et al* (2013) was implemented in TOPAS MC to reproduce the experimental microdosimetric spectra published by Martino *et al* (2010). To reproduce the experimental conditions, we simulated a spherical TEPC detector filled with propane-based gas (C_3H_8 (55%), CO_2 (39.6%) and N_2 (5.4%)) equivalent to a sphere of tissue of $2.7 \mu\text{m}$ in diameter.

We computed microdosimetric specific energy spectra at various depths along the beam directions. To validate our simulations, prior studies have already confirmed the accuracy of the simulated lineal energy spectra at three distinct positions: the entrance, Bragg-peak, and tail through experimental comparisons (Martino *et al* 2010, Burigo *et al* 2013, Zhu *et al* 2019). In the context of the SOBP, we conducted simulations with a sample size of 10^7 primaries for each position along the beam axis. We employed the HSG cell line to evaluate cell survival and the RBE depth curve, using 200 kV x-ray as the reference radiation source ($\alpha_X = 0.19 \text{ Gy}^{-1}$ and $\beta_X = 0.05 \text{ Gy}^{-2}$).

2.3.4. Cell survival and RBE assessment in a patient case

Predicting the cell survival fraction and RBE within the patient's anatomy involved a two-step process. First, we utilized the MONAS extension to create lookup tables (LUTs) of radiobiological parameters α and β for each model and proton beam energy. Then, we incorporated the MONAS LUTs into the TOPAS Monte Carlo particle transport algorithm to score the survival fraction and RBE in each voxel of the patient. To construct the LUTs, we irradiated a sphere of $1 \mu\text{m}$ of radius made of water with monoenergetic proton beams at different energies (from 0.1 to 300 MeV), and we scored the cell survival fraction with the MONAS extension. We fitted each survival curve with the LQ model, and we determined the α and β coefficients. Using the TOPAS particle transport algorithm, we created a novel scorer to calculate the mixed-field α_{mix} and β_{mix} for each voxel of the patient scoring mesh starting from the LUTs of monoenergetic beams. In particular, for each step s of primary and secondary protons inside the voxel v , we registered the kinetic energy of the particle ($E_{v,s}$) and the energy deposited along the step plus the energy released to secondary δ -rays ($dE_{v,s}$) (Cortés-Giraldo and Carabe 2015). As standard, the α_{mix} and β_{mix} are thus calculated as a weighted sum of α and β for the monoenergetic beam, (Zaider and Rossi 1980)

$$\alpha_{\text{mix}} = \frac{\sum_{s=1}^{N_s} dE_{v,s} \alpha(E_{v,s})}{\sum_{s=1}^{N_s} dE_{v,s}} \quad (6)$$

$$\sqrt{\beta}_{\text{mix}} = \frac{\sum_{s=1}^{N_s} dE_{v,s} \sqrt{\beta(E_{v,s})}}{\sum_{s=1}^{N_s} dE_{v,s}}. \quad (7)$$

To show the applicability of this approach in real patient irradiation, we simulated in TOPAS a head and neck treatment plan, optimized with the Eclipse treatment planning system (Varian Medical Systems, Palo Alto, CA) at the Dwoskin Proton therapy center (University of Miami). The plan comprises 2 coplanar fields at 30 and 60-degree gantry angles and a third noncoplanar at 30 degrees gantry and couch angle at 300 degrees. All fields employed a range shifter of 57 mm of water equivalent thickness. A uniform biological dose of 60 Gy (RBE) in 30 fractions was prescribed to the target using a constant RBE equal to 1.1.

We estimated the cell survival fraction and the dose-dependent RBE with the abovementioned approach. The radiobiological parameters for the reference radiation were $\alpha_X = 0.19 \text{ Gy}^{-1}$ and $\beta_X = 0.05 \text{ Gy}^{-2}$ for HSG cell line.

To compare our findings, we repeated the same analysis using the mSMKM based on the amorphous track description of radiation energy description at the microscopic scale (Inaniwa and Kanematsu 2018), which is the version currently used in carbon ion therapy. To generate the dose-averaged specific energies per event $\bar{z}_{d,D}$ and $\bar{z}_{d,D}^*$ imparted to the domain, and to the cell nucleus, $\bar{z}_{n,D}$, we employed the *Survival toolkit* code (Manganaro *et al* 2018). The resulting cell survival fraction and RBE are described in (Inaniwa and Kanematsu 2018).

3. Results

3.1. Radiobiological parameters

Table 2 reports the MKM and GSM² parameters that give the best fit for the *in vitro* cell-survival data of the HSG cell line when irradiated with ^{12}C and ^3He ion beams. Figure 3 shows the experimental cell survival fraction, as taken from the PIDE dataset, (Friedrich *et al* 2013), for the HSG cell line, compared to the corresponding

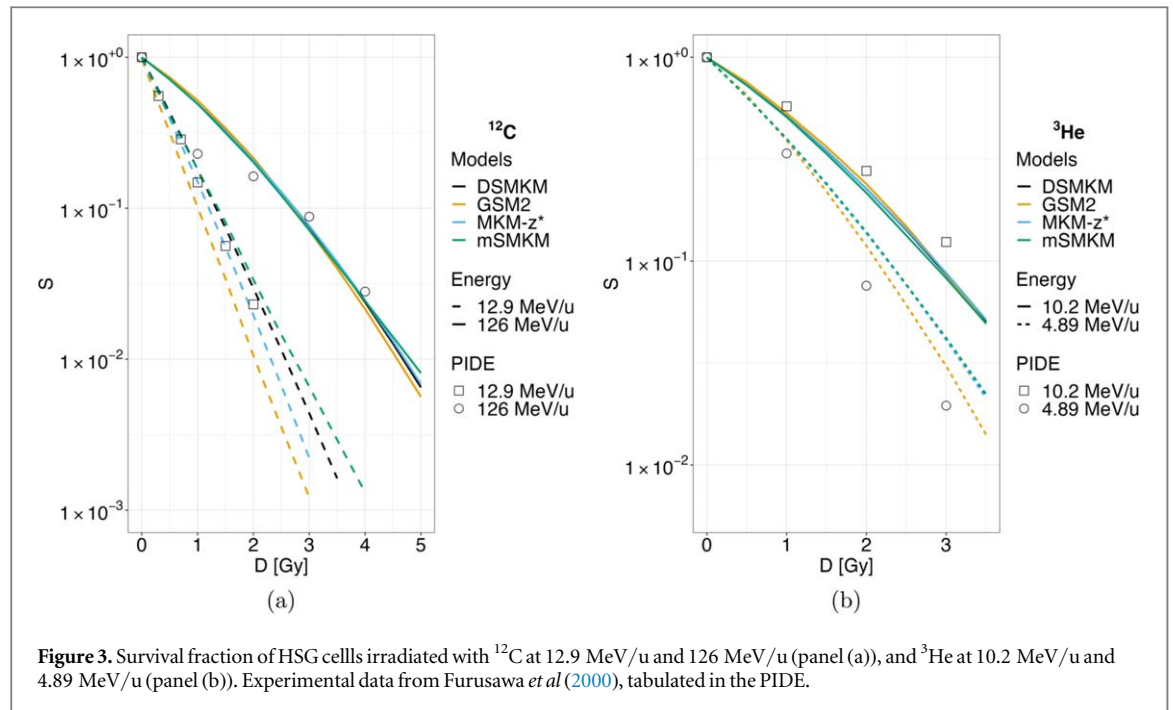


Table 2. MKM and GSM² model parameters for human salivary gland cell line. Experimental data are taken from the PIDE dataset, (Friedrich *et al* 2013).

	HSG				
	MKM-z*	DSMKM	mSMKM	GSM ²	
α_0 [Gy ⁻¹]	0.19	0.16	0.16	a [h ⁻¹]	0.037
β_0 [Gy ⁻²]	0.07	0.08	0.08	b [h ⁻¹]	0.182
γ_0 [keV/ μm]	150	—	—	r [h ⁻¹]	3.641
R_d [μm]	0.44	0.46	0.46	R_d [μm]	0.80
R_n [μm]	—	8.0	8.0	R_n [μm]	5.0

predicted cell survival curves using the four radiobiological models with parameters as given in table 2. All radiobiological models agree with the HSG *in vitro* cell survival curves for both carbon and helium ions.

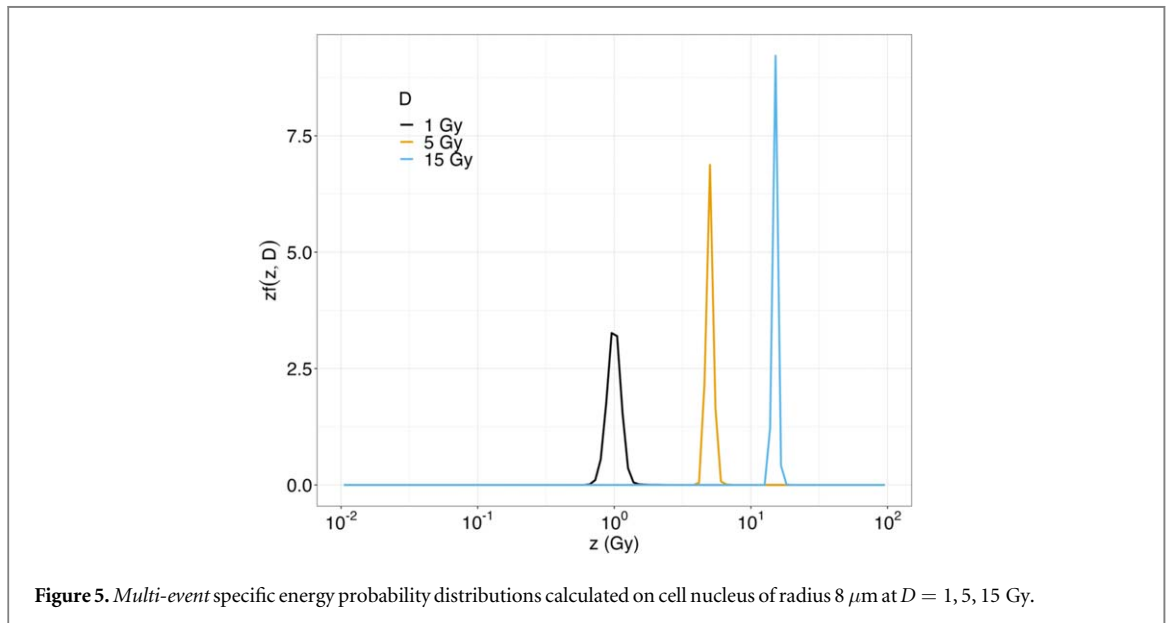
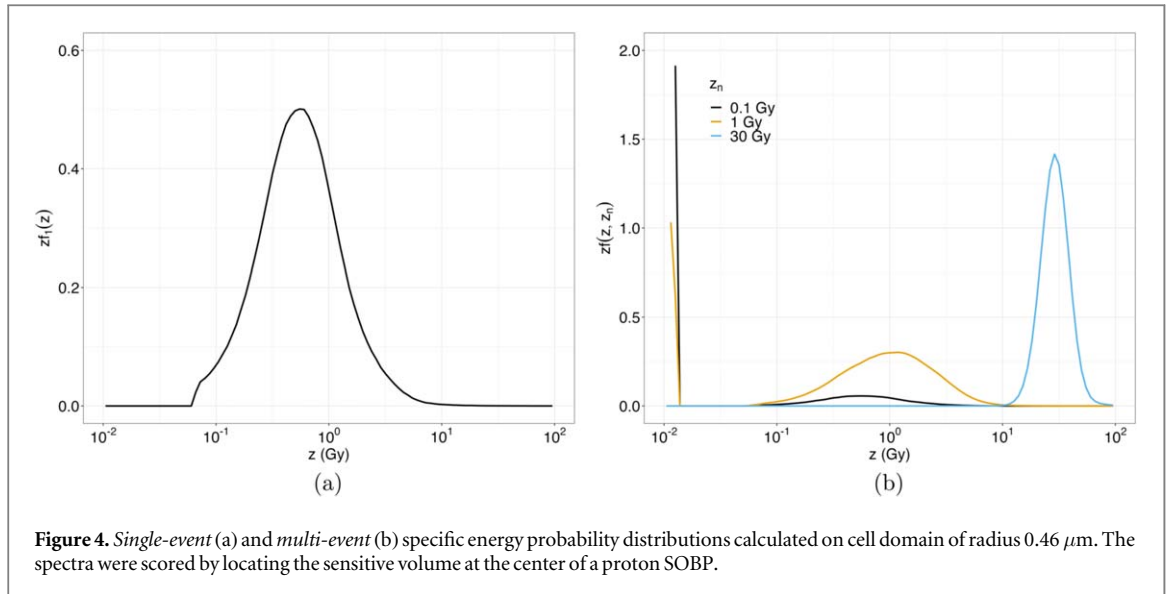
Regarding the fitted MKM parameters, given a new description of the physics of the radiation field employed in this study, all parameters have been recalibrated due to a discrepancy between cell survival experimental results and prediction using parameter values reported in the original papers. In particular, in Kase *et al* (2006), the MKM-z* parameters extrapolated directly from microdosimetric measurements of y_D and from *in vitro* HSG cell survival data are reported to be $\alpha_0 = 0.13 \text{ Gy}^{-1}$, $\beta = 0.05 \text{ Gy}^{-2}$. Absolute values of α_0 and β do not agree with our fit; nevertheless, the α/β ratio and domain radius are consistent with (Kase *et al* 2006). Further, DSMKM and mSMKM parameters are different from the originals, (Sato and Furusawa 2012, Inaniwa and Kanematsu 2018), but nevertheless, the difference in absolute value is moderate.

At last, concerning GSM², coherently with Missiaggia *et al* (2023b), only a , b , and r parameters were fitted, whereas domain and cell nucleus radius were set *a priori*. This is done to avoid overfitting.

3.2. Specific energy spectra

The novel specific energy scorer implemented in this work allows calculating the *single-* and *multi-event* probability distributions, both at the domain and cell nucleus scales, that is, in the order of 1 micron and 10 microns, respectively. Figure 4 shows the *single-event* $z f_1(z)$ and *multi-event* $z f(z, z_n)$ distributions computed at different averages doses $z_n = 0.1, 1$ and 30 Gy for a cell domain radius equal to 0.46 μm , chosen as the representative domain sizes for the DSMKM and the mSMKM. These spectra were calculated by locating the TEPC active volume at the center of the SOBP proton beam described in section 2.3.2.

The single-event distribution $z f_1(z)$ preserves a similar shape as the corresponding $y f(y)$ distribution, as could be expected from equation (2). On the contrary, the shape of the *multi-event* distribution changes significantly as a function of the dose delivered to the cell domain z_n . In particular, to lower doses, e.g. $z_n = 0.1$ and 1 Gy, it corresponds to a higher probability of null energy deposition in the domain due to the case of no



tracks hitting the target. This phenomenon is evident by the high peak at $z = 0 \text{ Gy}$. As the dose z_n increases, since the average value of Poisson distribution is proportional to z_n , the probability of scoring zero tracks vanishes, and consequently, the peak at null z disappears. All three multi-event distributions have an average value equal to z_n , and furthermore, at higher z_n the distribution is uni-modal and peaked at $z = z_n$ with a Gaussian-like shape.

The $zf(z, D)$ distribution at the cell nucleus scale, with a radius of $8 \mu\text{m}$, as a function of macroscopic dose $D = 1, 5, 15 \text{ Gy}$ is shown in figure 5. As before, the spectrum is generated by an SOBP proton beam. The *multi-event* distribution has a uni-modal Gaussian-like shape peaked at $z = D$ even at a low dose of $D = 1 \text{ Gy}$.

3.3. Cell survival and RBE for a proton Spread-out Bragg-peak

Cell survival fraction and RBE were calculated using MKM formulations and GSM^2 along the beam axis using experimentally validated microdosimetric spectra, (Missiaggia *et al* 2023a), as described in section 2.3.2. The physical 3D dose distribution was simulated in the water phantom using a voxel size of $1 \times 1 \times 1 \text{ mm}^3$ and normalized to 1.8 Gy at the center of SOBP to obtain a biological dose of 2 Gy(RBE) for constant RBE equal to 1.1.

Figure 6 panel (a) shows the depth survival curve compared to the physical dose. All models predict a similar trend: the survival is higher at the plateau, around 0.7, and drops to a minimum in the SOBP, where the survival remains constant at around 0.5. At the distal edge of the SOBP, the survival fraction raises again to a similar value

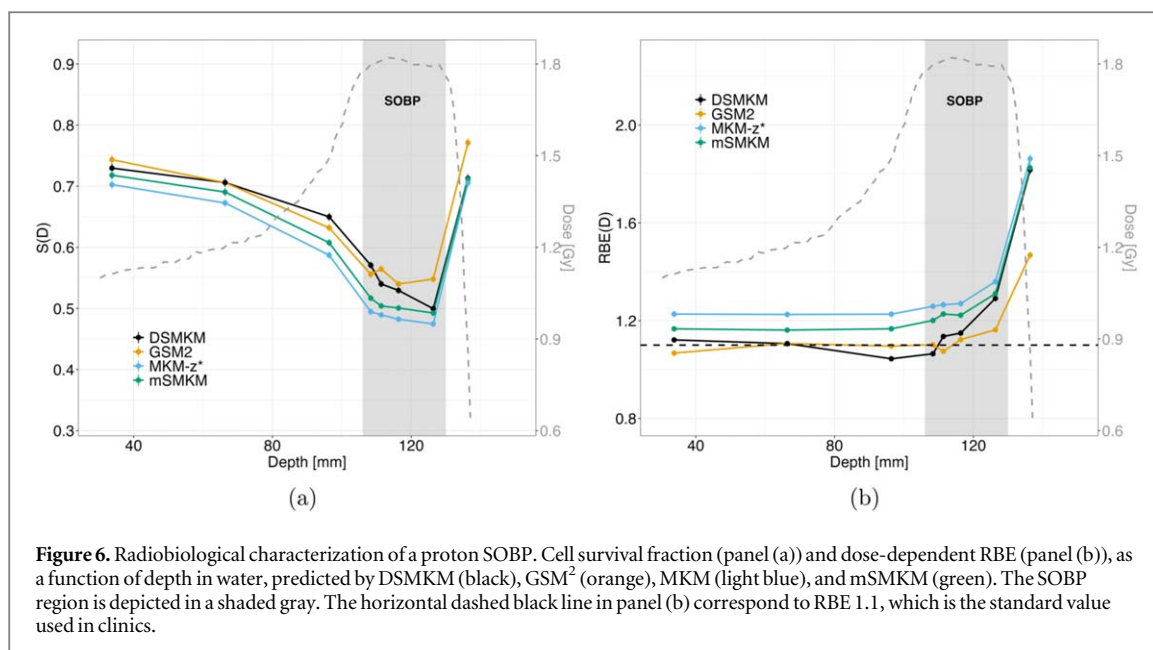


Figure 6. Radiobiological characterization of a proton SOBP. Cell survival fraction (panel (a)) and dose-dependent RBE (panel (b)), as a function of depth in water, predicted by DSMKM (black), GSM^2 (orange), MKM (light blue), and mSMKM (green). The SOBP region is depicted in a shaded gray. The horizontal dashed black line in panel (b) correspond to RBE 1.1, which is the standard value used in clinics.

Table 3. Cell survival fraction, $S(D)$, and $RBE(D)$ calculated with MKM formulations and GSM^2 for HSG cell line. The values are reported at three relevant water depths of the proton SOBP and ^{12}C -ion Bragg peak: plateau (34 mm), mid-SOBP (116 mm), and distal penumbra (136 mm) for SOBP; plateau (52.1 mm), Bragg peak (170 mm), and distal penumbra (277.1 mm). The values refer to the center of TEPC detector.

	1H Plateau		^{12}C Plateau	
	$S(D)$	$RBE(D)$	$S(D)$	$RBE(D)$
GSM^2	0.74 ± 0.03	1.06 ± 0.05	0.76 ± 0.04	2.29 ± 0.08
MKM- z^*	0.70 ± 0.02	1.22 ± 0.04	0.77 ± 0.04	2.22 ± 0.08
mSMKM	0.69 ± 0.02	1.16 ± 0.04	0.77 ± 0.04	2.20 ± 0.07
DSMKM	0.73 ± 0.03	1.12 ± 0.05	0.76 ± 0.04	2.44 ± 0.09
	1H mid-SOBP		^{12}C Bragg Peak	
	$S(D)$	$RBE(D)$	$S(D)$	$RBE(D)$
GSM^2	0.54 ± 0.02	1.12 ± 0.05	0.22 ± 0.01	2.94 ± 0.09
MKM- z^*	0.48 ± 0.01	1.27 ± 0.03	0.22 ± 0.01	2.94 ± 0.09
mSMKM	0.50 ± 0.01	1.22 ± 0.03	0.22 ± 0.01	2.94 ± 0.09
DSMKM	0.53 ± 0.02	1.15 ± 0.05	0.22 ± 0.01	3.04 ± 0.10
	1H Distal		^{12}C Tail	
	$S(D)$	$RBE(D)$	$S(D)$	$RBE(D)$
GSM^2	0.77 ± 0.07	1.47 ± 0.08	0.98 ± 0.07	1.51 ± 0.11
MKM- z^*	0.70 ± 0.04	1.86 ± 0.07	0.97 ± 0.07	2.04 ± 0.08
mSMKM	0.71 ± 0.04	1.82 ± 0.07	0.97 ± 0.07	1.95 ± 0.08
DSMKM	0.72 ± 0.07	1.81 ± 0.09	0.97 ± 0.07	2.09 ± 0.10

as the plateau. However, quantitative differences between the considered models are appreciable. The MKM- z^* and mSMKM formulations predict cell survival fractions systematically lower than GSM^2 in all regions. The DSMKM shows comparable survival fraction values with GSM^2 in the plateau up to the mid-SOBP, while in the distal region, GSM^2 predicts a slightly higher cell survival. Dose-dependent cell survivals were further used to calculate RBE according to equation (5). All the models predict an RBE higher than 1 for all depths, figure 6 panel (b). In addition, all models show a constant RBE trend as a function of penetration depth with a value between 1.1 and 1.2 in the plateau and a sharp increase in the distal edge of the field. Table 3 reports the survival fraction and RBE values, along with statistical errors, at three water depths: plateau (34 mm), middle SOBP (116 mm), and distal edge (136 mm).

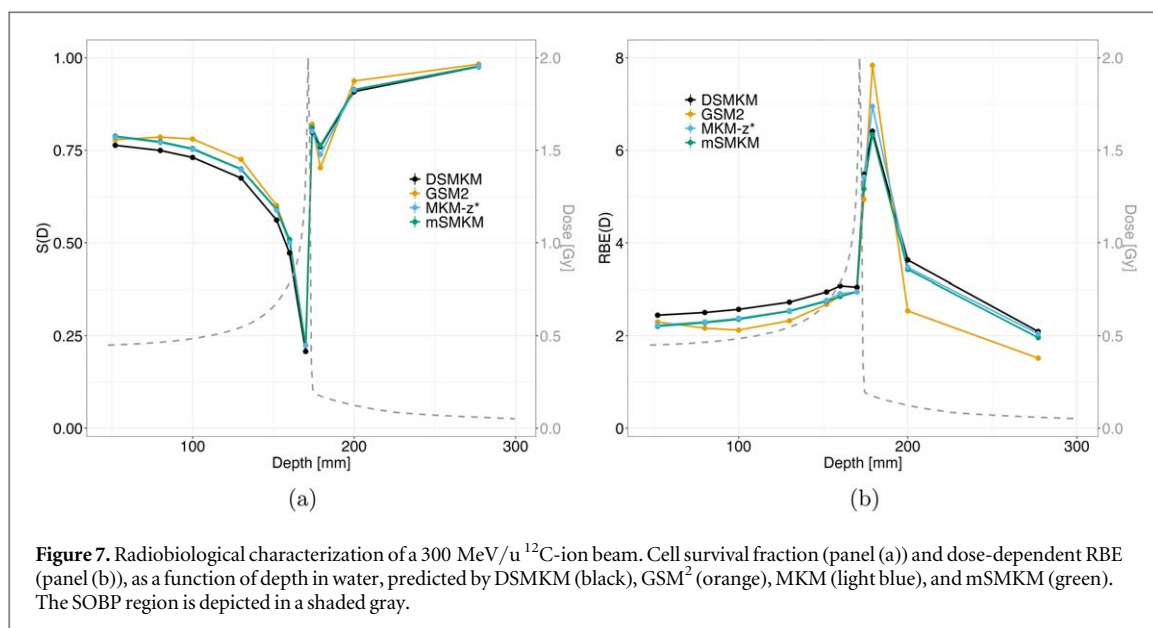


Figure 7. Radiobiological characterization of a 300 MeV/u ^{12}C -ion beam. Cell survival fraction (panel (a)) and dose-dependent RBE (panel (b)), as a function of depth in water, predicted by DSMKM (black), GSM 2 (orange), MKM (light blue), and mSMKM (green). The SOBP region is depicted in a shaded gray.

3.4. Cell survival and RBE for a 300 MeV/u ^{12}C -ion beam

Figure 7 illustrates the depth survival curve and RBE compared to the physical dose. The dose calculations were performed within a voxel size of $1 \times 1 \times 1 \text{ mm}^3$ and were normalized to 2 Gy at the Bragg peak. In the context of the spread-out Bragg peak (SOBP), all models consistently predict a higher cell survival in the plateau region, averaging at 0.76 ± 0.01 . This survival fraction decreases at the Bragg peak, reaching a minimum of 0.22 ± 0.01 . As we move far out-of-field, the survival fraction increases to 0.98 ± 0.07 .

The dose-dependent RBE of ^{12}C -ion beams is notably higher than that of proton RBE at all water depths. In the plateau region, all models converge on an average RBE value of 2.3 ± 0.1 , which sharply escalates to 6.9 ± 0.6 immediately after the Bragg peak. In the dose tail, situated far out-of-field, RBE values decrease to 1.9 ± 0.3 .

Table 2 presents the survival fraction and RBE values, along with their associated statistical errors, at three distinct water depths: plateau (52.1 mm), Bragg peak (170 mm), and dose tail (277.1 mm). We must note that we chose the simulation point at a water depth of 170 mm to represent the Bragg peak region. While in Zhu *et al* (2019), the Bragg peak region has been identified at a water depth of 179.1 mm, our simulations indicate that the Bragg peak is located at $171 \pm 1 \text{ mm}$ water depth, which is consistent with the findings (Burigo *et al* 2013). Thus, we have maintained consistency with our simulation results. Previous research has indicated that the peak in RBE for ^{12}C -ion beams is located a few millimeters downstream of the Bragg peak (Tommasino *et al* 2015). However, the substantial size of the spherical TEPC, measuring 1.27 cm in diameter, and the high sensitivity of microdosimetric spectra near the Bragg peak region could account for the peak in RBE being situated at 7 mm from the dose Bragg peak.

3.5. MONAS application to a patient case

To estimate a 3D spatial distribution of cell survival and RBE for a patient case, we calculated lookup tables (LUTs) of radiobiological parameters α and β for protons specific to the HSG cell line. We incorporated the LUTs within the TOPAS Monte Carlo algorithm and simulated a treatment plan, calculating the 3D spatial distributions of dose-dependent cell survival and RBE. To benchmark our results, we also included the mSMKM with amorphous track (mSMKM-AT), a validated radiobiological model for Carbon ion therapy, (Inaniwa and Kanematsu 2018). The 2D spatial distribution of cell survival fraction is plotted in figure 8 for GSM 2 (panel (c)), and mSMKM-AT (panel (a)) as a benchmark to the current state-of-the-art of MKM clinical application (tuned for carbon ion therapy). The two models agree in the shape of $S(D)$ distribution where a minimum (color map hot region) of the cell survival fraction is estimated in the Clinical Target Volume (CTV) and a few millimeters in the surrounding volume. By comparing the monodimensional depth-survival curves (panel (e)), large differences are evident among the models. MONAS-based MKM formulations predict the lowest $S(D)$ values (0.46 ± 0.03 on average in CTV), while GSM 2 and mSMKM-AT predict an average cell survival fraction of 0.52 ± 0.07 and 0.55 ± 0.04 , respectively.

The RBE 2D map displayed in panels (b) and (d) exhibits similar patterns: both the mSMKM-AT and GSM 2 are characterized by a notable increase in RBE values in the distal region of the therapeutic field, specifically at beam angles of 30 and 60 degrees. mSMKM-AT 2D distribution shows a wider dark red region (RBE values above 1.5) compared to GSM 2 in the distal part of the CTV, while in the patient's entrance mSMKM-AT map has

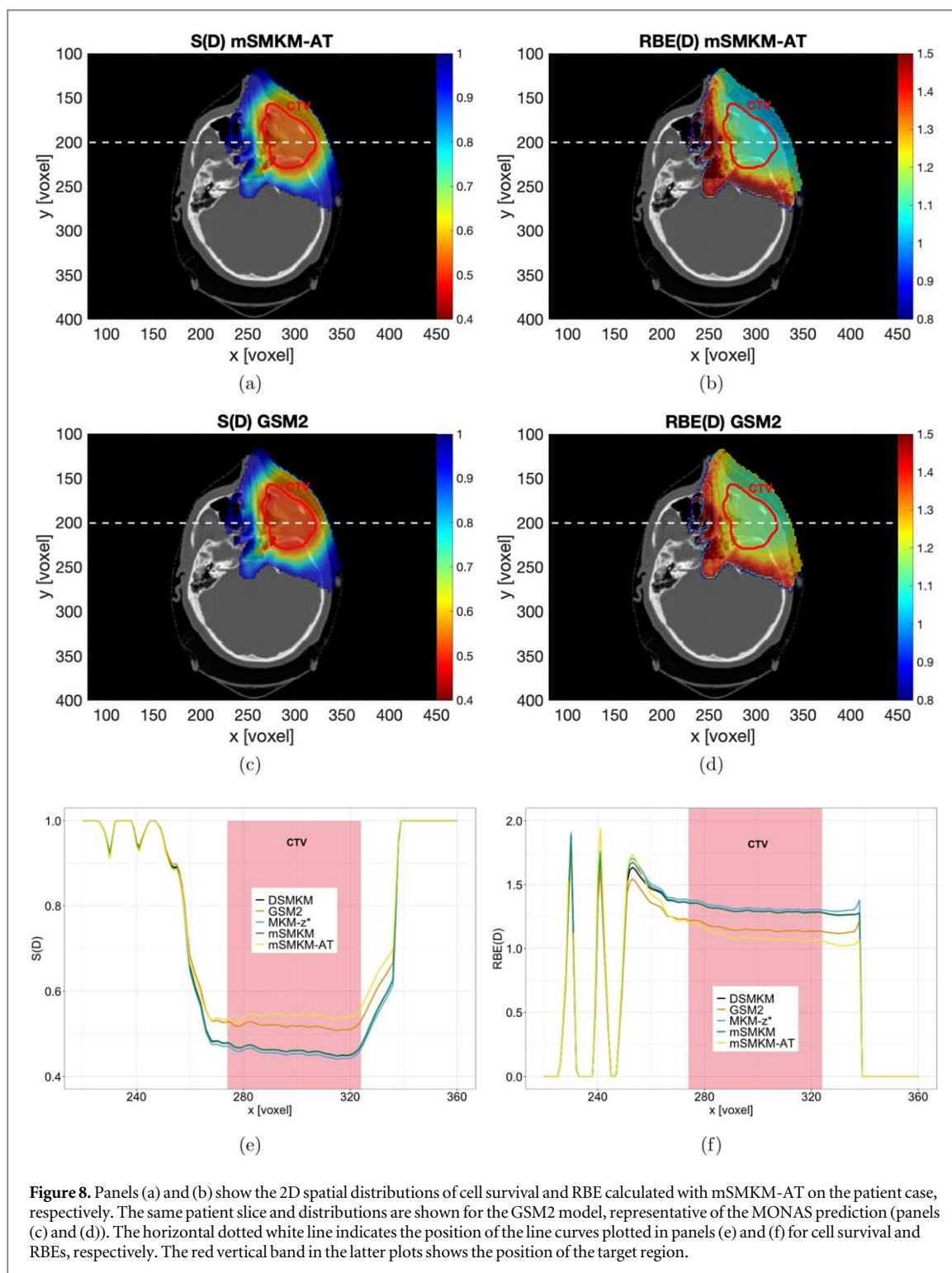


Figure 8. Panels (a) and (b) show the 2D spatial distributions of cell survival and RBE calculated with mSMKM-AT on the patient case, respectively. The same patient slice and distributions are shown for the GSM2 model, representative of the MONAS prediction (panels (c) and (d)). The horizontal dotted white line indicates the position of the line curves plotted in panels (e) and (f) for cell survival and RBEs, respectively. The red vertical band in the latter plots shows the position of the target region.

lower RBE values (blue colormap). As shown in the depth-RBE curve (panel (f)), MKM models from MONAS code predict RBE values systematically higher than GSM² and mSMKM-AT both at the beam entrance and in the distal region (from 1.3 to 1.6). GSM² model predicts RBE values lower than the MKM formulations from around 1.1 at the entrance, up to 1.5 downstream of the CTV. The same holds for mSMKM-AT, which shows RBE values around 1 at the entrance, exceeding GSM² in distal reaching RBEs of around 1.7. In figure 8 panel (f) all models shows two RBE peaks for voxel indices blow 240 on the x-axis. These values correspond to the distal out-of-field region of the beam, where the dose and the density are low due to the presence of the nasal cavities. In figure 8 panel (e), we observe cell survival values slightly higher than 0.9 in the same region. Since we are calculating the dose-dependent RBE, combining these cell survival spikes and the low dose values (which serve as the denominator in the RBE calculation) generates artifacts in the RBE distribution.

Although the inter-model differences in absolute values of the survival S and RBE, both MONAS-based and mSMKM-AT models show the same spatial distribution characteristics. Inside the target volume, S and RBEs remain constant and sharply increase at the distal edges of the fields where most organs at risk are located.

4. Discussion

In this work, we presented the MONAS toolkit, a TOPAS MC extension that combines accurate Monte Carlo simulations of microdosimetric distributions with microdosimetry-based models for predicting cell survival and RBE. MONAS provides a powerful tool to bridge the gap between a microdosimetric description of a radiation field, the biological evaluation of radiation effects, and its implementation in the clinical practice of proton beam therapy.

To show MONAS applications, we presented two examples: (i) the radiobiological characterization of a SOBP, and (ii) the calculation of the RBE spatial distribution for a real patient's treatment with protons. In figure 6, we showed that MONAS can estimate the cell survival fraction and RBEs from experimentally validated spectra, predicting a trend consistent with previous works (Kase *et al* 2006, Tran *et al* 2017). In this context, it is important to emphasize that most of the research paper on protons and heavier ions focuses on RBE_{10} , which is the ratio of reference radiation and ion dose giving the 10% survival fraction (Tran *et al* 2017, Debrot *et al* 2018, Bianchi *et al* 2020, Conte *et al* 2020). The RBE_{10} represents a universally accepted radiobiological endpoint, allowing thus a comparison of different radiobiological experiments. However, when considering clinical applications, it becomes more meaningful to examine a dose-dependent RBE, i.e. the RBE associated with the dose specifically absorbed by each voxel of the treatment plan. This critical information enables direct estimation of the treatment plan's biological effectiveness. The presented MONAS extension, which is directly linked to TOPAS, offers a rapid assessment of the MC-based dose-dependent RBE, which can have an impact both in clinical scenarios and in experimental radiobiology.

Using the complete range of microdosimetric spectrum as the input for radiobiological models emphasized the need to recalibrate the model parameters, as outlined in table 1, to accurately fit the MONAS cell survival curves with the existing experimental data. Figure 3 shows a good agreement between MONAS predictions and the experimental *in vitro* data at different irradiation conditions. Furthermore, the new set of parameters is consistent with parameters already published for the MKM (Kase *et al* 2006, Sato and Furusawa 2012, Inaniwa and Kanematsu 2018) in terms of the order of magnitude of the cell domain and nucleus radii, as well as the α - β absolute values. The MONAS toolkit thus further allows testing the robustness of the model parameter against experiments. In MONAS, all microdosimetric values are evaluated using the entire microdosimetric distribution (figures 4 and 5), which can be validated by direct comparison with the experimental y -spectra measured with commercial microdosimetric detectors. As a result, the MONAS toolkit provides a comprehensive framework for validating the entire radiobiological workflow, encompassing the simulation of the radiation field's physical properties and the direct estimation of its biological impact. This is achieved by utilizing microdosimetric quantities and cell survival experiments directly calibrated against experimental data, ensuring accuracy and reliability in assessing biological effectiveness.

The radiobiological models implemented in our code use domain radii smaller than $1\ \mu\text{m}$, a scale where a condensed history Monte Carlo might not be accurate. However, we primarily employed two sizes of scoring spheres: a $1\ \mu\text{m}$ radius sphere made of water and a $6.35\ \text{mm}$ radius sphere made of tissue-equivalent gas. Notably, studies by Zhu *et al* (2019), Bianchi *et al* (2023), Missiaggia *et al* (2023a) have demonstrated that microdosimetric spectra simulated with a TEPC detector align well with experimental data. The $1\ \mu\text{m}$ radius water sphere was used to construct the LUTs and replicate the PIDE cell survival data. As shown in figure SM.1 of the supplementary materials, the $6.35\ \text{mm}$ radius sphere made of tissue-equivalent gas and the $1\ \mu\text{m}$ produce identical microdosimetric spectra, which are used by our models to compute the cell survival curve. It is worth noticing that all the radiobiological use domain and nucleus radii that do not match the experimental or simulation active volume sphere. Therefore, we adopted a rescaling approach using the z - y relation: $z = \frac{0.16}{\rho\pi r^2}y$. This procedure, as employed in previous works (Kase *et al* 2006, 2013), allowed us to simulate microdosimetric spectra in larger geometries than the actual domain scale, providing valuable insights into the biological effects.

The second main application of MONAS is the RBE evaluation in a real patient case. In figure 8, we show the 3D spatial distribution of cell survival fraction and RBE values calculated for proton treatment of a head and neck tumor. The results for a complex beam and patient's geometry follow the same trend exhibited in figure 6 from the SOBP: RBE hot spots are observed at the distal edge of the field, where most of the organs at risk are located (e.g. salivary glands, oral cavity, optical nerves). We used the MONAS extension to generate LUTs of α and β coefficients for monoenergetic proton beams and eventually assess the biological effectiveness of a mixed-energy beam averaging α and β values. The RBE evaluated in the present paper is calculated considering only the contribution from primary and secondary protons, but it can be extended to include other secondary ions by

adding LUTs for alpha, carbons, and oxygen ions. This could increase the accuracy of the estimated RBE values, especially at the field-edge and out-of-field, where a non-negligible contribution to the radiation field is given by high-LET radiation such as alpha particles (Missiaggia *et al* 2023a). The application of MONAS in a real patient case represents a significant advancement in integrating a detailed microdosimetric description of the radiation field into treatment planning systems. These LUTs can be incorporated into a particle tracking Monte Carlo toolkit to estimate a three-dimensional map of cell survival fraction and RBE within a mixed-field radiation treatment plan.

While using LUTs does not fully address the computational challenge of simulating the complete microdosimetric distribution in all voxels, we propose a fundamental step into using microdosimetric information in proton and ion therapy. LUTs have been generated by simulating the entire microdosimetry distribution of monoenergetic beams, which were then used as input for the radiobiological models to estimate the cell survival fraction. Therefore, the intrinsic stochastic nature of energy deposition at the micron scale is considered in the final LUT values. Using pre-calculated α and β values that are loaded during the particle simulation in patients does not increase the treatment plan computation time. The time required by TOPAS MC to calculate α_{mix} and $\sqrt{\beta_{\text{mix}}}$ in each voxel of the patient is comparable to a similar volumetric scorer already implemented in TOPAS (e.g. *ProtonLET* Cortés-Giraldo and Carabe 2015, Granville and Sawakuchi 2015). This feature is of great significance in the proposed methodology because it enables the inclusion of our LUTs in clinical Monte Carlo treatment planning systems without causing a slowdown in computational time for treatment plan calculations. Indeed, a significant enhancement to this analysis could involve the creation of LUTs for different cell lines, each specifically assigned to a patient's organ. This approach would enable the calculation of cell-line-dependent RBE within the patient's anatomical context, thus accounting for the varying radiosensitivity of different clinical structures.

Our findings reveal that there is a clear inter-model variability in the absolute values of cell survival and, thus, in RBE values observed both in SOBP characterization and in the patient simulation, as seen in figures 6–8. Figures 8 panels (e)–(f) exhibit significant differences between the MKM models and GSM² in the CTV region, being further the mSMKM-AT closer to the GSM² prediction. Differences in the models stem from the fact that they all have different foundations and include different stochasticities. In addition, deviations in the predictions of RBE have already been verified in the literature when comparing the MKM with the LEM, (Monini *et al* 2019, Bellinzona *et al* 2021b). Furthermore, the predictions made by the implemented models exhibit consistent trends, with GSM² showing a higher predicted survival probability within the tumor compared to all versions of MKM. In the context of heavy ion beam irradiation, as depicted in figure 7, the variations between different models are less pronounced than in the case of proton irradiation. However, GSM² still exhibits deviations from MKM. In the scenario of high LET particles, the assumption that DNA damages follow a Poisson distribution is, in general, believed not to be valid. One notable strength of the GSM² model lies in its capacity to avoid assuming any Poisson distribution for both lethal and sub-lethal damages, a common practice in dealing with high-LET radiation energy deposition. This inherent distinction between MKM formulations and GSM² can lead to discrepancies between models, particularly in regions beyond the field of the heavy ion beam. The primary objective of this study is to present a proof-of-principle regarding the key features of MONAS, without imposing assumptions on the model's parameters. The strength of our toolkit lies in the ability to customize each model's parameters and cell line-specific settings. However, we provided a set of potential parameters that yield radiobiological results consistent with the *in vitro* data presented in figure 3. Further investigations will be conducted to calculate the model parameters that best fit a larger sample of experimental cell survival curves at various irradiation conditions. This analysis highlights the importance of determining precise model parameters that have a significant impact on the absolute values of cell survival fractions and, consequently, RBE. Furthermore, all models predict an RBE that significantly differs from the constant value used in the clinic. GSM² and the DSMKM calculate an RBE value close to 1.1 only in the plateau, while all the models show a sharp increase in the RBE in the distal region. This increase in the RBE could have an impact on the organs at risk located right after the tumor, for which a significant underestimation of RBE could lead to toxicities.

Microdosimetry is proving to be extremely valuable in clinical applications for several compelling reasons, surpassing the traditional use of LET values and providing a more reliable and experimentally measurable, as demonstrated in numerous campaigns conducted over the years, (Kase *et al* 2006, Tran *et al* 2018, Bianchi *et al* 2020, Missiaggia *et al* 2020, Lee *et al* 2021, Magrin *et al* 2023, Missiaggia *et al* 2023a), radiation quality description. Moreover, microdosimetry naturally includes the geometry of the sensitive volume in the measured spectra, providing information that not only considers the stochastic nature of energy deposition but also incorporates specific geometric considerations of the studied volume. This eliminates any potential uncertainty in interpreting the analyzed spectra and quantities. Because of the several LET definitions, it can be challenging to discern whether the value indicates the track average or the dose average. Additionally, different LET scorers are commonly used, and including only primary particles or both primary and secondary particles in the scorer

can completely change the physical significance of the resulting values and the estimation of the biological effect (Grassberger and Paganetti 2011, Bellinzona *et al* 2021a, Kalholm *et al* 2021). This becomes particularly problematic in the out-of-field regions, where the radiation field is mixed, short-track particles can play a significant role, and LET may not accurately characterize the radiation quality (Grün *et al* 2019). On the other hand, microdosimetry offers comprehensive information that allows for a precise assessment of all the physical processes involved, enabling a more accurate estimation of the biological effects.

Therefore, radiotherapy clinical practice can greatly benefit from consistently and rigorously evaluating treatment plans based on microdosimetry. In the past, the computational effort required for calculating microdosimetry quantities in treatment plans has been a hindrance to its practical implementation in the clinic. However, with advancements in computational power and the effective simplification methods demonstrated in this study, clinicians can now improve the prescribed treatment plans by incorporating microdosimetric considerations allowing for a more robust estimation of the plan's biological effectiveness.

5. Conclusions

In this work, we presented a novel TOPAS MC extension, MONAS: MicrOdosimetry-based modelliNg for RBE ASsessment, which allows the user to evaluate dose-dependent cell survival curves and RBE with the most used microdosimetry-based radiobiological models: three MKM formulations (saturation corrected MKM (MKM- z^*) (Kase *et al* 2006), double stochastic MKM (DSMKM) (Sato and Furusawa 2012) and the modified Stochastic MKM (mSMKM) (Inaniwa and Kanematsu 2018) and the GSM² model, (Cordoni *et al* 2021, 2022b).

MONAS wraps the already published TOPAS microdosimetric extensions to evaluate the single- and multi-event specific energy (z) distributions at different micrometric scales. Full microdosimetric distributions are then used as input for both MKM and GSM² models. This approach showed intrinsic differences in microdosimetric radiation characterization with respect to the amorphous track structure model used in the latest MKM formulations. Therefore, we recalculated the model parameter that best fit the radiobiological experiments for the HSG cell line. To show the main MONAS applications, we reproduced experimental microdosimetric spectra from a passively scattered SOB. We used the MONAS code to assess cell survival fraction and RBE as a function of proton penetration depth. Our findings are consistent with the well-known RBE trend, which presents a steep increase in the distal edge of the field. Furthermore, we were able to assess the high inter-model variability on the absolute RBE values thus quantifying a radiobiological uncertainty in proton plans in addition to other physical uncertainties.

The applicability of the MONAS toolkit can be further extended to a radiobiological analysis of treatment plans. We showed that it is possible to generate radiobiological parameter look-up tables which can be combined with the Monte Carlo toolkit for computing RBE maps on patients and therapeutic beam geometries. We showed an example of cell survival and RBE predictions on a real head and neck proton therapy plan delivered at the Dvoskin Proton Therapy Center at the University of Miami. The results have been compared to the mSMKM model based on the amorphous track structure model, as recently developed in (Inaniwa and Kanematsu 2018), representing one of the most used models in carbon ion therapy. Despite the variability in RBE absolute values, all the models showed a reasonable RBE trend as a function of beam penetration depth.

In conclusion, the MONAS extension offers a comprehensive microdosimetric framework for assessing the biological effect of radiation in both research and clinical environments. MONAS could be a key tool to include a detailed microdosimetric description of radiation field into treatment planning systems for variable RBE calculations.

Data availability statement

All data that support the findings of this study are included within the article (and any supplementary information files).

ORCID iDs

Giorgio Cartechini  <https://orcid.org/0000-0003-2092-7279>

Marta Missiaggia  <https://orcid.org/0000-0002-2896-0981>

Emanuele Scifoni  <https://orcid.org/0000-0003-1851-5152>

Chiara La Tessa  <https://orcid.org/0000-0001-5742-6772>

Francesco G Cordoni  <https://orcid.org/0000-0002-1295-7884>

References

- Agostinelli S et al 2003 Geant4a simulation toolkit *Nucl. Instrum. Methods Phys. Res. A* **506** 250–303
- Attili A, Scifoni E and Tommasino F 2022 Modelling the hprt-gene mutation induction of particle beams: systematic in vitro data collection, analysis and microdosimetric kinetic model implementation *Phys. Med. Biol.* **67** 1–15
- Baiocco G, Bartzsch S, Conte V, Friedrich T, Jakob B, Tartas A, Villagrasa C and Prise KM 2022 A matter of space: how the spatial heterogeneity in energy deposition determines the biological outcome of radiation exposure *Radiat. Environ. Biophys.* **61** 545–59
- Baratto-Roldán A, Bertolet A, Baiocco G, Carabe A and Cortés-Giraldo M A 2021 Microdosimetry and dose-averaged let calculations of protons in liquid water: a novel geant4-dna application *Front. Phys.* **9** 1–13
- Bellinzona E V et al 2021a Biological impact of target fragments on proton treatment plans: An analysis based on the current cross-section data and a full mixed field approach *Cancers* **13** 4768
- Bellinzona V, Cordonni F, Missiaggia M, Tommasino F, Scifoni E, La Tessa C and Attili A 2021b Linking microdosimetric measurements to biological effectiveness in ion beam therapy: a review of theoretical aspects of mkm and other models *Front. Phys.* **8** 1–28
- Bianchi A et al 2020 Microdosimetry with a sealed mini-tepc and a silicon telescope at a clinical proton sobp of catana *Radiat. Phys. Chem.* **171** 1–7
- Bianchi A, Selva A, Reniers B, Vanhavere F and Conte V 2022 Topas simulations of the response of a mini-tepc: benchmark with experimental data *Phys. Med. Biol.*
- Bianchi A, Selva A, Reniers B, Vanhavere F and Conte V 2023 Topas simulations of the response of a mini-tepc: benchmark with experimental data *Phys. Med. Biol.* **68** 1–12
- Bradley P, Rosenfeld A and Zaider M 2001 Solid state microdosimetry *Nucl. Instrum. Methods Phys. Res. B* **184** 135–57
- Burigo L, Pshenichnov I, Mishustin I and Bleicher M 2013 Microdosimetry of radiation field from a therapeutic 12c beam in water: a study with geant4 toolkit *Nucl. Instrum. Methods Phys. Res. B* **310** 37–53
- Cartechini G 2023 *Monas gitlab repository*
- Chatterjee A and Schaefer H 1976 Microdosimetric structure of heavy ion tracks in tissue *Radiat. Environ. Biophys.* **13** 215–27
- Conte V et al 2020 Microdosimetry of a therapeutic proton beam with a mini-tepc and a microplus-bridge detector for rbe assessment *Phys. Med. Biol.* **65** 1–22
- Conte V, Selva A, Colautti P, Hilgers G, Rabus H, Bantsar A, Pietrzak M and Pszona S 2018 Nanodosimetry: towards a new concept of radiation quality *Radiat. Prot. Dosim.* **180** 150–6
- Cordonni F, Missiaggia M, Attili A, Welford S, Scifoni E and La Tessa C 2021 Generalized stochastic microdosimetric model: the main formulation *Phys. Rev. E* **103** 1–29
- Cordonni F G, Missiaggia M, La Tessa C and Scifoni E 2022a Multiple levels of stochasticity accounted for in different radiation biophysical models: from physics to biology *Int. J. Radiat. Biol.* 1–16
- Cordonni F G, Missiaggia M, Scifoni E and La Tessa C 2022b Cell survival computation via the generalized stochastic microdosimetric model (gsm2): I. The theoretical framework *Radiat. Res.* **197** 218–32
- Cortés-Giraldo M and Carabe A 2015 A critical study of different Monte Carlo scoring methods of dose average linear-energy-transfer maps calculated in voxelized geometries irradiated with clinical proton beams *Phys. Med. Biol.* **60** 1–262645
- De Nardo L, Cesari V, Donà G, Magrin G, Colautti P, Conte V and Tornielli G 2004 Mini-tepcs for radiation therapy *Radiat. Prot. Dosim.* **108** 345–52
- Debrot E et al 2018 Soi microdosimetry and modified mkm for evaluation of relative biological effectiveness for a passive proton therapy radiation field *Phys. Med. Biol.* **63** 1–10
- Durante M, Orecchia R and Loeffler J S 2017 Charged-particle therapy in cancer: clinical uses and future perspectives *Nat. Rev. Clin. Oncol.* **14** 483–95
- Friedrich T et al 2018 Dna damage interactions on both nanometer and micrometer scale determine overall cellular damage *Sci. Rep.* **8** 1–10
- Friedrich T, Scholz U, Elsässer T, Durante M and Scholz M 2013 Systematic analysis of rbe and related quantities using a database of cell survival experiments with ion beam irradiation *J. Radiat. Res.* **54** 494–514
- Furusawa Y, Fukutsu K, Aoki M, Itsukaichi H, Eguchi-Kasai K, Ohara H, Yatagai F, Kanai T and Ando K 2000 Inactivation of aerobic and hypoxic cells from three different cell lines by accelerated 3he-, 12c- and 20ne-ion beams *Radiat. Res.* **154** 485–96
- Garty G, Schulte R, Shchemelinin S, Leloup C, Assaf G, Breskin A, Chechik R, Bashkirov V, Milligan J and Grosswendt B 2010 A nanodosimetric model of radiation-induced clustered dna damage yields *Phys. Med. Biol.* **55** 761–81
- Granville D A and Sawakuchi G O 2015 Comparison of linear energy transfer scoring techniques in monte carlo simulations of proton beams *Phys. Med. Biol.* **60** 283–91
- Grassberger C and Paganetti H 2011 Elevated let components in clinical proton beams *Phys. Med. Biol.* **56** 6677–91
- Grün R, Friedrich T, Traneus E and Scholz M 2019 Is the dose-averaged let a reliable predictor for the relative biological effectiveness? *Med. Phys.* **46** 1064–74
- Hawkins R 1996 A microdosimetric-kinetic model of cell death from exposure to ionizing radiation of any let, with experimental and clinical applications *Int. J. Radiat. Biol.* **69** 739–55
- Hawkins R B 1994 A statistical theory of cell killing by radiation of varying linear energy transfer *Radiat. Res.* **140** 366–74
- Hawkins R B 2003 A microdosimetric-kinetic model for the effect of non-poisson distribution of lethal lesions on the variation of rbe with let *Radiat. Res.* **160** 61–9
- Inaniwa T, Furukawa T, Kase Y, Matsufuji N, Toshito T, Matsumoto Y, Furusawa Y and Noda K 2010 Treatment planning for a scanned carbon beam with a modified microdosimetric kinetic model *Phys. Med. Biol.* **55** 6721–37
- Inaniwa T and Kanematsu N 2018 Adaptation of stochastic microdosimetric kinetic model for charged-particle therapy treatment planning *Phys. Med. Biol.* **63** 1–17095011
- Inaniwa T, Suzuki M, Furukawa T, Kase Y, Kanematsu N, Shirai T and Hawkins R B 2013 Effects of dose-delivery time structure on biological effectiveness for therapeutic carbon-ion beams evaluated with microdosimetric kinetic model *Radiat. Res.* **180** 44–59
- Jäkel O, Bert C, Fossati P and Kamada T 2016 ICRU report 93: prescribing, recording, and reporting light ion beam therapy *J. ICRU* **16** 37–58
- Jarlskog C Z and Paganetti H 2008 Physics settings for using the geant4 toolkit in proton therapy *IEEE Trans. Nucl. Sci.* **55** 1018–25
- Kalhofer F, Grzanka L, Traneus E and Bassler N 2021 A systematic review on the usage of averaged let in radiation biology for particle therapy *Radiother. Oncol.* **161** 211–21
- Kase Y, Kanai T, Matsufuji N, Furusawa Y, Elsässer T and Scholz M 2007 Biophysical calculation of cell survival probabilities using amorphous track structure models for heavy-ion irradiation *Phys. Med. Biol.* **53** 37–59
- Kase Y, Kanai T, Matsumoto Y, Furusawa Y, Okamoto H, Asaba T, Sakama M and Shinoda H 2006 Microdosimetric measurements and estimation of human cell survival for heavy-ion beams *Radiat. Res.* **166** 629–38

- Kase Y, Yamashita W, Matsufuji N, Takada K, Sakae T, Furusawa Y, Yamashita H and Murayama S 2013 Microdosimetric calculation of relative biological effectiveness for design of therapeutic proton beams *J. Radiat. Res.* **54** 485–93
- Kiefer J and Straaten H 1986 A model of ion track structure based on classical collision dynamics (radiobiology application) *Phys. Med. Biol.* **31** 1201–9
- Lee S H et al 2021 Estimating the biological effects of helium, carbon, oxygen, and neon ion beams using 3d silicon microdosimeters *Phys. Med. Biol.* **66** 1–14
- Loeffler J S and Durante M 2013 Charged particle therapy optimization, challenges and future directions *Nat. Rev. Clin. Oncol.* **10** 411–24
- Magrin G, Palmans H, Stock M and Georg D 2023 State-of-the-art and potential of experimental microdosimetry in ion-beam therapy *Radiother. Oncol.* **182** 109586
- Mairani A et al 2022 Roadmap: helium ion therapy *Phys. Med. Biol.* **67** 1–63
- Manganaro L, Russo G, Bourhaleb F, Fausti F, Giordanengo S, Monaco V, Sacchi R, Vignati A, Cirio R and Attili A 2018 'survival': a simulation toolkit introducing a modular approach for radiobiological evaluations in ion beam therapy *Phys. Med. Biol.* **63** 1–8
- Manganaro L, Russo G, Cirio R, Dalmaso F, Giordanengo S, Monaco V, Muraro S, Sacchi R, Vignati A and Attili A 2017 A monte carlo approach to the microdosimetric kinetic model to account for dose rate time structure effects in ion beam therapy with application in treatment planning simulations *Med. Phys.* **44** 1577–89
- Martino G, Durante M and Schardt D 2010 Microdosimetry measurements characterizing the radiation fields of 300 mev/u 12c and 185 mev/u 7li pencil beams stopping in water *Phys. Med. Biol.* **55** 3441–9
- McMahon S J 2018 The linear quadratic model: usage, interpretation and challenges *Phys. Med. Biol.* **64** 1–24
- Mein S, Klein C, Kopp B, Magro G, Harrabi S, Karger C P, Haberer T, Debus J, Abdollahi A, Dokic I et al 2020 Assessment of rbe-weighted dose models for carbon ion therapy toward modernization of clinical practice at hit: *in vitro* and in patients *Int. J. Radiat. Oncol. * Biol. * Phys.* **108** 779–91
- Missiaggia M, Cartechini G, Scifoni E, Rovituso M, Tommasino F, Verroi E, Durante M and La Tessa C 2020 Microdosimetric measurements as a tool to assess potential in-field and out-of-field toxicity regions in proton therapy *Phys. Med. Biol.* **65** 1–16
- Missiaggia M, Cartechini G, Tommasino F, Scifoni E and La Tessa C 2023a Investigation of in-field and out-of-field radiation quality with microdosimetry and its impact on relative biological effectiveness in proton therapy *Int. J. Radiat. Oncol. * Biol. * Phys.* **115** 1269–82
- Missiaggia M, Cordoni F G, Scifoni E and La Tessa C 2023b Cell survival computation via the generalized stochastic microdosimetric model (GSM2): II. Numerical results *Radiat. Res.* **0** 1–12
- Missiaggia M et al 2021 A novel hybrid microdosimeter for radiation field characterization based on the tissue equivalent proportional counter detector and low gain avalanche detectors tracker: a feasibility study *Front. Phys.* **8** 1–16
- Monini C, Alphonse G, Rodriguez-Lafrasse C, Testa É and Beuve M 2019 Comparison of biophysical models with experimental data for three cell lines in response to irradiation with monoenergetic ions *Phys. Imaging Radiat. Oncol.* **12** 17–21
- Paganetti H 2014 Relative biological effectiveness (rbe) values for proton beam therapy. variations as a function of biological endpoint, dose, and linear energy transfer *Phys. Med. Biol.* **59** 419–72
- Paganetti H and Goitein M 2000 Radiobiological significance of beamline dependent proton energy distributions in a spread-out bragg peak *Med. Phys.* **27** 1119–26
- Perl J, Shin J, Schumann J, Faddegon B and Paganetti H 2012 Topas: an innovative proton monte carlo platform for research and clinical applications *Med. Phys.* **39** 6818–37
- Rabus H and Nettelbeck H 2011 Nanodosimetry: bridging the gap to radiation biophysics *Radiat. Meas.* **46** 1522–8
- Rosenfeld A B 2016 Novel detectors for silicon based microdosimetry, their concepts and applications *Nucl. Instrum. Methods Phys. Res. A* **809** 156–70
- Sato T and Furusawa Y 2012 Cell survival fraction estimation based on the probability densities of domain and cell nucleus specific energies using improved microdosimetric kinetic models *Radiat. Res.* **178** 341–56
- Sato T, Kase Y, Watanabe R, Niita K and Sihver L 2009 Biological dose estimation for charged-particle therapy using an improved phits code coupled with a microdosimetric kinetic model *Radiat. Res.* **171** 107–17
- Sato T et al 2013 Particle and heavy ion transport code system, phits, version 2.52 *J. Nucl. Sci. Technol.* **50** 913–23
- Sato T, Watanabe R and Niita K 2006 Development of a calculation method for estimating specific energy distribution in complex radiation fields *Radiat. Prot. Dosim.* **122** 41–5
- Scholz M, Jakob B and Taucher-Scholz G 2001 Direct evidence for the spatial correlation between individual particle traversals and localized cdkn1a (p21) response induced by high-let radiation *Radiat. Res.* **156** 558–63
- Selva A, Colautti P and Conte V 2020 Nanodosimetry of light ions in targets of different size *Radiat. Phys. Chem.* **172** 1–7
- Tambas M et al 2022 Current practice in proton therapy delivery in adult cancer patients across europe *Radiother. Oncol.* **167** 7–13
- Tommasino F, Scifoni E and Durante M 2015 New ions for therapy *Int. J. Part. Ther.* **2** 428–38
- Tommasino F et al 2019 A new facility for proton radiobiology at the trento proton therapy centre: design and implementation *Phys. Med.* **58** 99–106
- Tran L T et al 2018 The relative biological effectiveness for carbon, nitrogen, and oxygen ion beams using passive and scanning techniques evaluated with fully 3D silicon microdosimeters *Med. Phys.* **45** 2299–308
- Tran L T et al 2017 Characterization of proton pencil beam scanning and passive beam using a high spatial resolution solid-state microdosimeter *Med. Phys.* **44** 6085–95
- Zaider M, Rossi B H H and Zaider M 1996 *Microdosimetry and its Applications* (Springer)
- Zaider M and Rossi H 1980 The synergistic effects of different radiations *Radiat. Res.* **73** 2–9
- Zhu H et al 2019 The microdosimetric extension in topas: development and comparison with published data *Phys. Med. Biol.* **64** 1–15